Rare Metal Materials and Engineering
Volume 55, Issue 5, May 2026
Available online at www.rmme.ac.cn

Science Press

Cite this article as: Wang Kangan, Li Muxi, Hou Hua, et al. Effect of Gradient Layer Thickness on Anti-penetration Properties of 2024 Al/TC4 Laminated Composites[J]. Rare Metal Materials and Engineering, 2026, 55(05): 1170-1183. DOI: https://doi.org/10.12442/j.issn.1002-185X.20240842.

ARTICLE

Effect of Gradient Layer Thickness on Anti-penetration Properties of 2024 Al/TC4 Laminated Composites

Wang Kangan[1], Li Muxi[1], Hou Hua[1,2], Zhao Yuhong[1,3,4]

[1] Collaborative Innovation Center of Ministry of Education and Shanxi Province for High-Performance Al/Mg Alloy Materials, School of Materials Science and Engineering, North University of China, Taiyuan 030051, China; [2] School of Materials Science and Engineering, Taiyuan University of Science and Technology, Taiyuan 030024, China; [3] Beijing Advanced Innovation Center for Materials Genome Engineering, University of Science and Technology Beijing, Beijing 100083, China; [4] Institute for Materials Intelligent Technology, Liaoning Academy of Materials, Shenyang 110164, China

Abstract: A gradient structure was introduced into a metal laminated target plate, and the anti-penetration simulation of the gradient structure was compared with that of a uniform-layer-thickness target plate by finite element simulation. The analysis was verified by an impact experiment. Results show that the high-level thickness and appropriate percentage of Ti alloy at the upper side of the gradient structure provide greater impact resistance against the bullet, which increases the warhead breakage and enhances the anti-penetration performance. In addition, during the impact process, the stress is transmitted and reflected in the form of waves in each layer of the target plate, and the interaction between the compression and tension waves causes non-synergistic deformation of the target plate and leads to delamination. The gradient target plate takes penetration resistance a step further through the higher energy absorption rate and more consumption of the bullet kinetic energy. This research provides a theoretical basis for the application of gradient structures in metallic laminated armor.

Key words: gradient structure; laminated composites; finite element analysis; anti-penetration mechanism

1 Introduction

With the rapid development of rockets and armor-breaking shells, the traditional homogeneous armor of single structure is no longer able to withstand the metal jets and explosive impacts generated by advanced weapons. Laminated composite armor has a layered structure, so the physical properties between the layers are different, which can interfere with the stability of the metal jet of the projectile and sharply decrease the blast impact, thus reducing the armor-breaking ability of the projectile[1–3]. Therefore, laminated composite armor shows great potential in the field of armor protection. Among various metal laminated composite armors, Ti-Al laminated composites have received widespread attention due to their excellent properties, such as low density, high specific strength, and high impact resistance[4–7].

The unique laminated structure and the combination of multiple metals of metal laminated composites result in a high degree of designability[8–9]. Li et al[10] prepared TC4-2024 Al laminated composites with different layer thicknesses by discharge plasma sintering. The results showed that the tensile strength and plasticity of TC4-2024 Al laminated composites were increased with the increase in layer thickness. Zhang et al[11] found that the overall anti-penetration performance can be improved by optimizing the Ti layer thickness of Ti/Al_3Ti laminated composites based on the finite element method. The Ti/Al_3Ti laminated composites showed optimal anti-penetration performance when Ti content was 27.7vol%. Bai et al[12] prepared AZ31/Mg-Gd laminated composite sheets with different layer thickness ratios, and it was reported that the optimal bending and tensile properties were obtained with

Received date: May 26, 2025
Foundation item: National Defense Basic Scientific Research Program of China (JCKY2020408B002, WDZC2022-12); Key Research and Development Program of Shanxi Province (202102050201011, 202202050201014); Fundamental Research Program of Shanxi Province (20210302124178, 20210302123061, 202103021224183)
Corresponding author: Zhao Yuhong, Ph. D., Professor, Collaborative Innovation Center of Ministry of Education and Shanxi Province for High-Performance Al/Mg Alloy Materials, School of Materials Science and Engineering, North University of China, Taiyuan 030051, P. R. China, E-mail: zhaoyuhong@nuc.edu.cn

the thickness ratio of AZ31 layer to Mg-Gd layer as 2∶1. In summary, the layer thickness variation has a significant effect on the mechanical properties of the laminated structure.

Gradient structures can enhance the anti-penetration performance of target plates and are mainly used in ceramic-metal composites. Wang et al[13] simulated the bullet resistance of B_4C/Al gradient armor and found that the penetration resistance of gradient armor against bullets was significantly better than that of homogeneous armor. Wang et al[14] dispersed ceramic particles in a gradient form in the $Al_{0.3}$CoCrFeNi matrix. The results show that the gradient structure leads to stronger anti-penetration properties under the condition of the same total volume fraction of ceramics. Zhang et al[15] prepared Ti/TiB-TiB_2 gradient composites by spark plasma sintering (SPS) combined with tape casting. High-speed impact tests showed that the Ti/TiB-TiB_2 gradient composites have excellent anti-penetration performance and penetration resistance against the secondary impact. In ceramic-metal composites, the introduction of a gradient structure has improved the anti-penetration properties of the target plates. However, the application of gradient structures mainly changes the matrix structure and does not change the layup structure.

Among the metal target plates, Zhang et al[16] prepared a magnesium alloy target plate with a gradient distribution of grain size using surface mechanical attrition treatment method. Although the anti-penetration performance was improved, the gradient structure of matrix remained, and the monolayer structure led to inferior resistance against the metal jets as well as blast impacts.

The gradient structure can effectively improve the anti-penetration performance of the target plate, and the layer thickness is also an important factor affecting the mechanical properties of the laminated structure. Combining the layer thickness with the gradient structure and changing the layup structure of the target plate into a gradient-thickness form may further improve the penetration resistance of the target plate. Shi et al[17] combined the gradient structure with layer thickness and introduced it into Ti/Al_3Ti laminated composite target plates. The results show that the anti-penetration properties of Ti/Al_3Ti laminated composite target plates with different gradient layup structures differ significantly. The composite target plate with forward gradient distribution has the optimal anti-penetration performance, and the anti-penetration performance is gradually enhanced with the increase in gradient variation. The influence mechanism is still obscure. Therefore, it is of great significance to clarify the mechanism of the anti-penetration performance of the gradient structure and to optimize the gradient structure for the improvement of overall anti-penetration performance of the target plate.

Numerical simulation can simulate physical experiments by computers and mathematical models to break through time and space constraints. Common numerical simulation methods include the phase field method[18–21], molecular dynamics[22–23], and finite element method[11,24–25]. In this research, the anti-penetration performance of 2024 Al/TC4 laminated composites with gradient layer thicknesses at different elastic velocities was investigated by computer simulation using the finite element method, and the performance was compared with that of the 2024 Al/TC4 laminated composites with uniform layer thickness. 2024 Al/TC4 laminated composites with uniform and gradient layer thicknesses were prepared by SPS, and impact experiments were conducted to verify and analyze the simulation results. The bullet residual velocity curves, morphological changes of the warhead and target plate, and the distribution of interlayer cracks and stresses in the anti-penetration process were analyzed in the simulation results. The underlying mechanism was discussed, which provided a theoretical basis for the application of gradient structure in the metal laminated armor.

2 Model Establishment

2.1 Finite element model

The simulation experiments used 2024 Al/TC4 laminated composites as well as tungsten alloy warheads as prototypes. SolidWorks modeling software was used to establish a three-dimensional solid model with the bullet length of 23 mm, bullet diameter of 6.15 mm, and target plate size of 100 mm (length)×100 mm (width)×11 mm (height). The bullet was perpendicular to the target plate intrusion. Considering the performance of the computer and to reduce the computing time, a 1/2 symmetric model was used, and meshing was performed in HyperMesh. The mesh model is shown in Fig. 1. The mesh was divided into a bullet model and a target plate model. The bullet mesh was divided by model segmentation, mesh mapping, symmetry, and other methods, and the common nodes were merged to make the bullet mesh as a whole. The target plate model was uniformly divided into 11 layers. Each layer existed independently with 1 mm in thickness, and the target plate grid size was 0.5 mm×0.5 mm×0.2 mm.

In order to investigate the anti-penetration performance of different target plates, gradient-layer-thickness and uniform-layer-thickness target plate models were established and compared with the simulation results obtained by LS-DYNA finite element software. Besides, the gradient-layer-thickness and uniform-layer-thickness target plates were denoted as gradient and uniform target plates, respectively. The total thickness, the number of layers, and the volume fraction occupied by titanium and aluminum were the same for the gradient and uniform target plates. The total thickness of the target plate was 11 mm, the total number of layers was 11, the

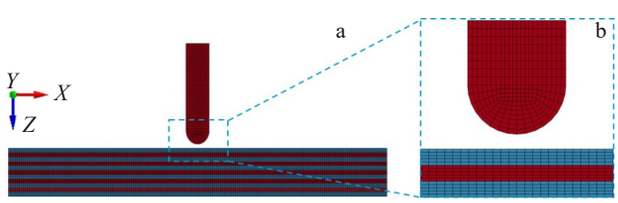

Fig.1 Schematic diagrams of anti-penetration modeling (a) and local enlargement of marked region in Fig.1a (b)

layer thickness of the uniform target plate was 1 mm, and the layer thickness variation of gradient target plate was 0.2 mm. Detailed thickness data are shown in Table 1. The arrangement of the TC4 layer and 2024 Al layer is shown in Fig. 2, where blue represents TC4 layer, and red represents 2024 Al layer. The TC4 layer of 1.8 mm in thickness in the gradient target plate is the bullet-responsive surface. The total thickness of TC4 layer in the gradient target plate was 6 mm, and the total thickness of 2024 Al was 5 mm. The total thickness of the TC4 layers and 2024 Al layers in the uniform target plate is the same as that of gradient target plate.

2.2 Model parameter

2.2.1 Constitutive model

Johnson-Cook model is a thermodynamic model[26–27] coupled with constitutive equation for high-rate deformations of many materials, including most metals[28], and the Johnson-Cook model was still valid at lower strain rates and even quasi-static states. Typical applications include explosive metal forming, ballistic penetration, and impact. Therefore, in this research, the Mat-Johnson-Cook constitutive model was used to describe the parameters of tungsten alloys, titanium alloys, and aluminum alloys[29].

The Johnson-Cook model consists of two main parts: the strength model and the failure model. The Johnson-Cook damage evolution[24] can be defined as follows:

$$D=\sum \Delta\varepsilon_p/\varepsilon_p^f \tag{1}$$

where D is the damage parameter; $\Delta\varepsilon_p$ is the effective plastic strain for one integration cycle; ε_p^f is the plastic strain at failure under gauge pressure. The specific expression of plastic strain at failure under gauge pressure[30] is as follows:

$$\varepsilon_p^f=(D_1+D_2\exp D_3\sigma^3)(1+D_4\ln\varepsilon^*)(1+D_5T^*) \tag{2}$$

where D_1, D_2, D_3, D_4, and D_5 are related damage parameters; σ is stress; ε^* is dimensionless strain; T^* is a similar temperature.

The larger the D value, the more serious the material damage. When D=1, the material fractures.

The Johnson-Cook model was used to calculate the flow stresses in material[30] by Eq.(3), as follows:

$$\sigma_{eq}=\left(A+B\varepsilon_{eq}^n\right)\left(1+C\ln\dot{\varepsilon}_{ep}^*\right)\left(1-T^{*m}\right) \tag{3}$$

where A represents the yield stress; B and n represent the strain hardening effect; C and m represent the strain rate constants; ε_{eq} is equivalent plastic strain; T^* is a similar temperature; $\dot{\varepsilon}_{eq}^*$ is the dimensionless plastic strain rate. This equation characterizes the effect of equivalent plastic strain, strain rate, and temperature on flow stress. Besides, T^* can be obtained by Eq.(4), as follows:

$$T^*=\frac{T-T_r}{T_m-T_r} \tag{4}$$

where T is temperature; T_r is room temperature; T_m is the melting point of the material. The Johnson-Cook model parameters of tungsten alloys, TC4, and 2024 Al are shown in Table 2[31–33].

2.2.2 Equation of state

In LS-DYNA software, when the Johnson-Cook constitutive model was used with solid units, it is necessary to incorporate the state equations. Therefore, the Gruneisen equation of state was adopted in this research, and the parameters of the Gruneisen equation of state for tungsten alloys, TC4, and 2024 Al are shown in Table 3[11], and the description of parameters is shown in Ref. [11]. The equation of state describes the relationship between various parameters of material, such as pressure, density, and temperature. The pressure of a compressed material[34] can be defined as follows:

$$P=\frac{\rho^0C^2\mu\left[1+\left(1-\frac{\gamma_0}{2}\right)\mu-\frac{\alpha}{2}\mu^2\right]}{\left[1-(S_1-1)\mu-S_2\frac{\mu^2}{\mu+1}-S_3\frac{\mu^3}{(\mu+1)^2}\right]^2}+(\gamma_0+\alpha\mu)E \tag{5}$$

where E is the internal energy per initial volume; C is the volumetric sound velocity of material; S_1, S_2, and S_3 are the equation of state coefficients; γ_0 is the Gruneisen constant; α is the first-order volume correction factor for γ_0; $\mu=(1/v)-1$ with v as the relative volume ($v=\rho/\rho_0$, where ρ is density, and ρ_0 is initial density).

2.2.3 Interfacial bonding and other parameters

Heterogeneous layer bonding of Al-Ti laminated composite relies on the intermetallic compound Al_3Ti generated during the preparation process. However, the thickness of Al_3Ti interfacial layer is usually less than 10 μm[35]. The thickness of titanium and 2024 Al layers in the Al-Ti laminated composites is at the millimeter level, and the finite element modeling cannot be combined with micron-sized meshes due to space and scale factors. Therefore, in this research, the Al_3Ti interface layer is neglected during the simulation of interfacial bonding through mesh-node contact as well as automatic-surface-to-surface-tiebreak method[36]. The interfacial bonding force between the titanium and aluminum layers was set as 107.5 MPa[37], and delamination of the aluminum and titanium layers occurs when the shear force applied at the interface during impact is greater than 107.5 MPa[38]. The contact

Table 1 Layer thickness of gradient target plate (mm)

Material	Layer					
	1st	2nd	3rd	4th	5th	6th
TC4	1.8	1.2	1.0	0.8	0.6	0.6
2024 Al	1.4	1.2	1.0	0.8	0.6	-

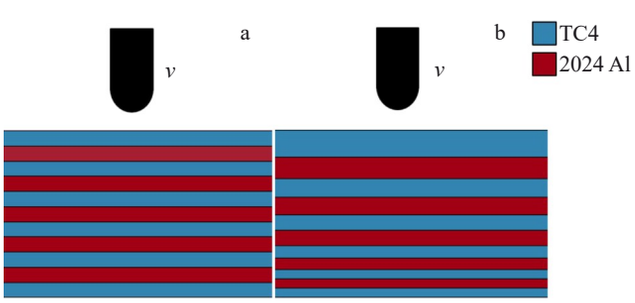

Fig.2 Schematic diagrams of uniform target plate (a) and gradient target plate (b)

Table 2 Parameters of Johnson-Cook constitutive models of different materials[31–33]

Parameter	Tungsten	TC4	2024 Al
Density, RO/g·cm^{-3}	17.7	4.45	2.79
Shear modulus, G/GPa	140	41.9	27.6
Young's modulus, E/GPa	310	113.8	71
Poisson's ratio, υ	0.3	0.34	0.33
Static yield strength, A/MPa	1506	1000	265
Strain hardening coefficient, B/MPa	177	845	426
Strain hardening exponent, n	0.12	0.58	0.34
Strain rate coefficient, C	0.016	0.014	0.015
Thermal softening exponent, m	1	0.753	1
Melt temperature, T_m/K	1498	1951	903
Room temperature, T_r/K	293	293	293
Damage constant, D_1	2	0.05	0.13
Damage constant, D_2	-	0.27	0.13
Damage constant, D_3	-	–0.48	–1.5
Damage constant, D_4	-	0.014	0.011
Damage constant, D_5	-	3.8	-

Table 3 Parameters of Gruneisen equation of state of different materials[11]

Material	Volumetric sound velocity, C/m·s^{-1}	Coefficient of equation of state, S_1	Gruneisen constant, γ_0	V_0
Tungsten	4030	1.240	1.54	1
TC4	5130	1.028	1.23	1
2024 Al	5328	1.338	2.00	1

between the warhead and each layer of the target plate is generated during the penetration process, and the contact relationship between the warhead and the target needs further investigation. In this research, contact-eroding-surface-to-surface contact[39] was adopted, which enables the bullet to re-establish contact with the next layer of the target plate after penetrating a single layer of the target plate. In this case, it is ensured that the bullet is in contact with all layers of the target plate during the penetration process[40].

The initial velocity of the bullet is set to an appropriate value that can ensure the bullet having sufficient kinetic energy through initial-velocity-generation method, and the direction of the initial velocity is consistent with that of the model. It is also necessary to set the solution time, time step, unit algorithm, and file output format of the model. Reasonable solution time and time step ensure a complete run of the model and reduce the chance of negative volume errors. The cell algorithm used for the 3D model is SECTION-SOLID, and the file output format is D3PLOT format to output the entire dynamic anti-penetration process.

2.2.4 Preparation of laminated composites

According to the impact model of uniform target plate, 6 pieces of TC4 foil of 1.0 mm in thickness and 5 pieces of 2024 Al foil of 1.0 mm in thickness were selected as the raw materials to constitute the uniform target plate. One piece of TC4 foil of 1.8, 1.2, 1.0, and 0.8 mm in thickness, two pieces of TC4 foil of 0.6 mm in thickness, and one piece of 2024 Al foil of 1.4, 1.2, 1.0, 0.8, and 0.6 mm were chosen as the raw materials for the preparation of the gradient target plate. Due to the size limitation of the prepared molds, the metal foil was cut into round foils with a diameter of 50 mm using an electrical discharge machining cutter, and the foil surface was slightly polished with sandpaper to remove burrs and oxidation layers. The surface grease of 2024 Al and TC4 foils was washed off by 10vol% NaOH and 10vol% HF solutions, respectively. The etched 2024 Al and TC4 foils were placed in anhydrous ethanol and subjected to ultrasonic vibration for 30 min to wash away surface impurities. Then, the treated foil was dried, and 5 pieces of 2024 Al foil and 6 pieces of TC4 foil were alternately stacked as a laminated structure and placed in the sintering furnace for SPS. The foils were compacted under a pressure of 5 MPa and heated to 550 ℃ in vacuum environment. After SPS for 90 min, 2024 Al/TC4 laminated composites were obtained. Fig. 3 shows the flow chart of the preparation process of 2024 Al/TC4 laminated composite.

3 Results

3.1 Residual velocity of bullet

To investigate the anti-penetration performance of target plates of different structures, different initial velocities of bullet (700 – 1200 m/s) were selected to impact the target plates. The residual velocity of bullet was calculated by LS-DYNA finite element software, and the results are shown in Fig. 4. It is found that when the initial velocity of bullet is

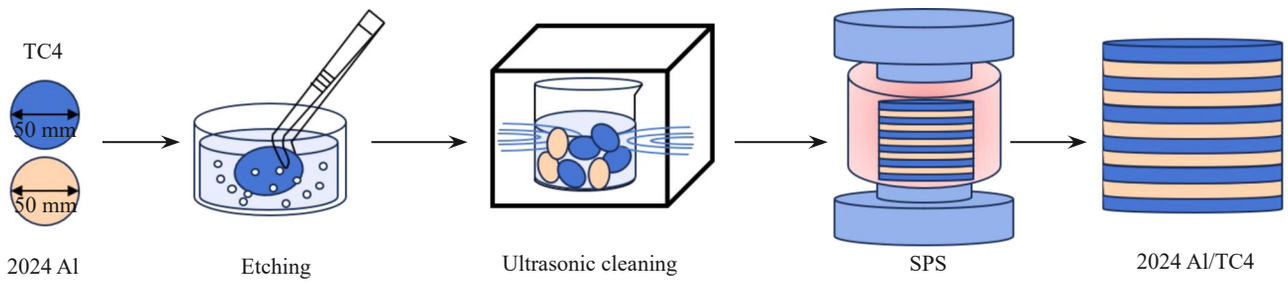

Fig.3 Flow chart of preparation process of 2024 Al/TC4 laminated composite

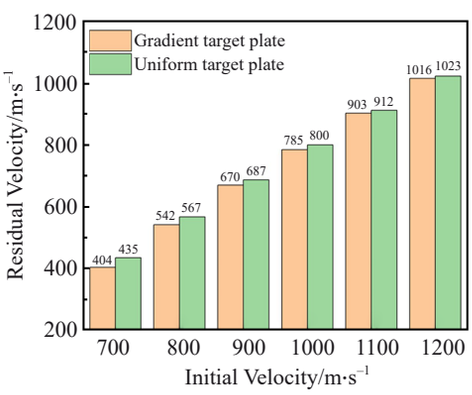

Fig.4 Residual velocity of bullets after penetrating gradient and uniform target plates

1200 m/s, the residual velocity of the bullet after penetrating the gradient target plate is 1016 m/s, which is slower than that after penetrating the uniform target plate by 7 m/s. When the initial velocity of the bullet reduces to 1000 m/s, the residual velocity of bullet after penetrating the gradient target plate is 15 m/s slower than that after penetrating the uniform target plate. When the initial velocity of the bullet further reduces to 700 m/s, the residual velocity difference is 31 m/s between gradient and uniform target plates after penetration. At the same initial velocity of bullet, both target plates are penetrated with the same thickness, the same number of layers, and the same volume fraction of titanium and aluminum. However, the residual velocity of the bullet is slower after penetrating the gradient target plate. As the initial velocity of the bullet decreases, the anti-penetration performance of the gradient target plate gradually increases, compared with that of uniform target plate. Therefore, it can be inferred that the anti-penetration performance of 2024 Al/TC4 laminated composites with gradient structure is superior to that of 2024 Al/TC4 laminated composites with uniform structure.

To gain a deeper understanding of the enhancement mechanism of anti-penetration performance of the gradient target plate, the velocity of the bullet impacting the gradient and uniform target plates with the initial velocity of bullet as 800 m/s was analyzed, and the results are shown in Fig. 5. It can be seen that the velocity curve in Fig. 5a has more curvature, the bullet velocity reduces more obviously, and the gradient structure has better anti-penetration performance, compared with that in Fig. 5b. Points A_1-E_1 in Fig. 5a and points A_2-E_2 in Fig. 5b correspond to the velocity of bullet at different moments. From 0 μs to 50 μs (A_1B_1 and A_2B_2 segments), the velocity of bullet impacting the gradient and uniform target plates decreases from 800 m/s to 668 and 700 m/s, respectively. The most significant decrease in bullet velocity occurs during this period, and the decrement of bullet velocity in the gradient target plate case is 32 m/s larger than that in the uniform target plate case. The longer the impacting duration, the less the decrement of bullet velocity. At 200 μs, the impact process is over, and the gradient target plate reduces the bullet velocity by 258 m/s, which is 25 m/s more than that caused by uniform target plate. According to these velocity analysis results, it can be inferred that the anti-penetration performance of gradient target plate is better than that of uniform target plate.

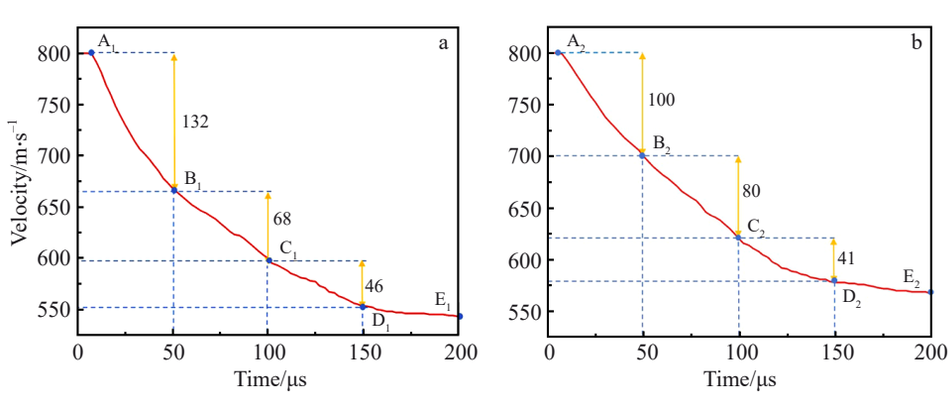

Fig.5 Velocity curves of bullet impacting gradient target plate (a) and uniform target plate (b)

3.2 Target plate shape

The deformation area of the target plate around the warhead and the bullet hole was analyzed, and the model morphologies are shown in Fig. 6. As shown in Fig. 6a_1–6a_2, the warheads touch the gradient and uniform target plates, no deformation occurs in both target plates, and the bullet velocity does not change. As shown in Fig. 6b_1, the third layer of the gradient target plate is penetrated, i. e., the TC4 layers of 2.5 mm in total thickness and the 2024 Al layers of 1.4 mm in total thickness are penetrated. As shown in Fig. 6b_2, 4 layers of uniform target plate are penetrated: TC4 layers of 2.0 mm in total thickness and 2024 Al layers of 2.0 mm in total thickness. Combined with the velocity curves of the bullet (Fig. 5) and the target plate morphology analysis at the moment of 50 μs, it is inferred that the velocity decrement of bullet is related to the thickness of the penetrated TC4 and 2024 Al layers. The penetration depth of the gradient target plate is 0.1 mm less than that of the uniform target plate at this time. The gradient target plate has 11 layers with a total thickness of 11.0 mm, and the total thickness of the first four layers of the gradient target plate reaches 5.6 mm, where the titanium content accounts for 50.0% of whole titanium content in the gradient target plate. On the contrary, the total thickness of the first four layers of the uniform target plate is 4.0 mm, and the titanium content accounts for 33.3% of whole titanium content in the uniform target plate. The layer thickness distribution of the gradient target plate results in a larger layer thickness and a higher percentage of titanium in the first four layers. In addition, the strength of TC4 alloy is higher than that of 2024 Al alloy. As a result, the bullet impacting the gradient target plate can slow down more significantly. At that moment, both the gradient and uniform target plates show bulging and interlayer cracking phenomena, and the gradient target plate shows more interlayer cracking.

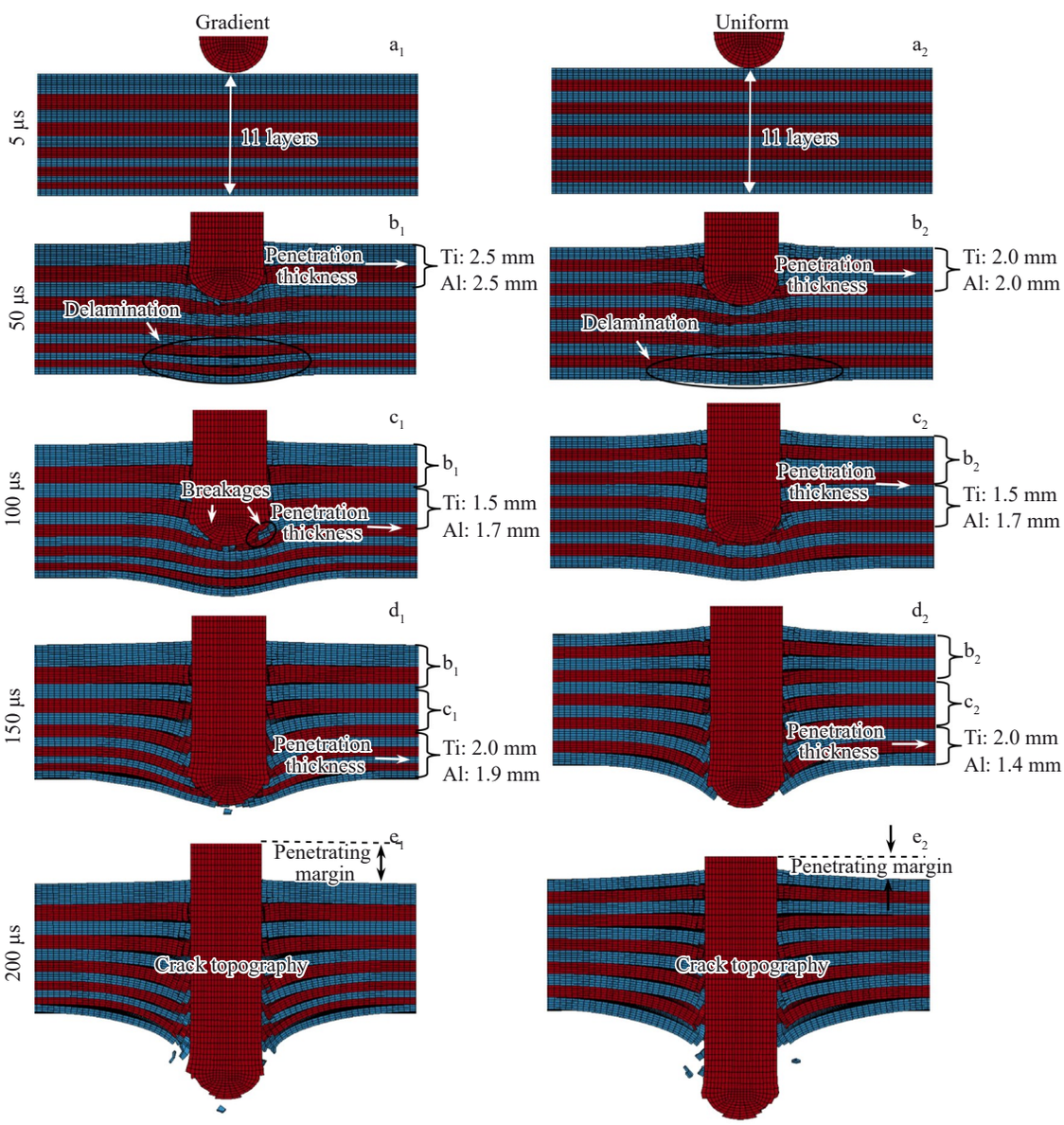

Fig.6 Model shapes of gradient target plate (a_1 – e_1) and uniform target plate (a_2 – e_2) during impacting at different moments: (a_1 – a_2) 5 μs; (b_1–b_2) 50 μs; (c_1–c_2) 100 μs; (d_1–d_2) 150 μs; (e_1–e_2) 200 μs

With deeper penetration, the gradient target plate is penetrated to the 6th layer at the moment of 100 μs, and the uniform target plate is penetrated to the 8th layer. During impacting from 50 μs to 100 μs, the bullet velocity decreases more rapidly in the uniform target plate, compared with that in the gradient target plate. This is because the bullet impacts the TC4 layer with thicker thickness in the uniform target plate during that period. Due to the extrusion influence of bullet, the deformation of the back plate is serious at this time, the interlayer cracking occurs in the middle layer of the gradient target plate and uniform target plate, and the warhead is broken, as marked by the black circles in Fig. 6c$_1$. The bullet penetrates all layers of the target plate at the moment of 150 μs, the interlayer cracking becomes more serious, and the 11th (TC4 alloy) of the gradient target plate is torn by the impact of warhead, as shown in Fig. 6d$_1$. The uniform target plate is almost punctured, and the 11th layer (TC4 alloy) is more severely torn, compared with that of the gradient target plate at the same moment. The gradient target plate is thicker in TC4 and 2024 Al layers for the upper layers, compared to the uniform target plate on the bullet-responsive side. Maximum reduction in bullet velocity occurs in the early stage throughout penetration process.

Although the 11th layer of the gradient target plate is not as thick as that of the uniform target plate, the kinetic energy of the bullet decreases obviously in the early penetration stage, indicating that the overall anti-penetration performance of the gradient target plate is better than that of the uniform target plate. At 200 μs, both the gradient target plate and the uniform target plate are completely penetrated. Compared with those in Fig. 6e$_2$, the size of the bullet hole in Fig. 6e$_1$ is larger, the degree of warhead breakage in Fig.6e$_1$ is more serious, and the remaining length of the bullet (penetrating margin) is larger. These results suggest that the gradient target plate has better penetration resistance. Because titanium and aluminum alloys have fine mechanical properties, local plastic deformation occurs in the metal target plate at the impact point, and no obvious fracture spalling occurs[41]. As the penetration depth increases, the target plate bottom flips downward severely, and the interlayer cracks are longer, which reflects the failure mechanism of the material[42].

3.3 Validation of simulation conclusions

Fig. 7 shows the uniform and gradient laminated composites prepared by SPS. TC4 layer and 2024 Al layer are stacked alternately for the uniform target plate, the layer thickness is uniform, and there is no obvious defect or damage at the interface, indicating that the interface is well combined.

To verify the simulation conclusions, anti-penetration experiments were performed. The experimental firearms selected 95-type automatic rifles with bullet of 5.8 mm in caliber, impact velocity of 800 m/s, and muzzle-to-target plate distance of 5 m. The surface and bottom of the sample were both subjected to impact. A laser velocimeter was installed at 3 m away from the muzzle and at 2 m behind the sample to record the initial and residual velocities of the bullets.

Recorded by the laser velocimeter, the initial velocities of the bullets impacting the uniform and gradient target plates are both 820 m/s. The residual velocity of the bullet impacting the uniform target plate is 510 m/s, and that impacting the gradient target plate is 476 m/s. The results show that the gradient target plate reduces bullet velocity more significantly, and the gradient target plate has superior anti-penetration properties. Fig. 8 shows the appearances of uniform and gradient target plates after penetration. The gradient target plate has no obvious deformation on the bullet-responsive surface, whereas the bottom side shows intense deformation and delamination phenomena. The damage morphologies are similar to the simulation results, which further illustrates the reliability of the simulation results. In addition, bending deformation occurs at the bottom side of the gradient target plate, and no obvious deformation occurs on the surface of the gradient target plate. This is because the upper TC4 layers are thicker, and the 2024 Al layer of the target plate can provide stronger deformation resistance. Unlike the gradient target

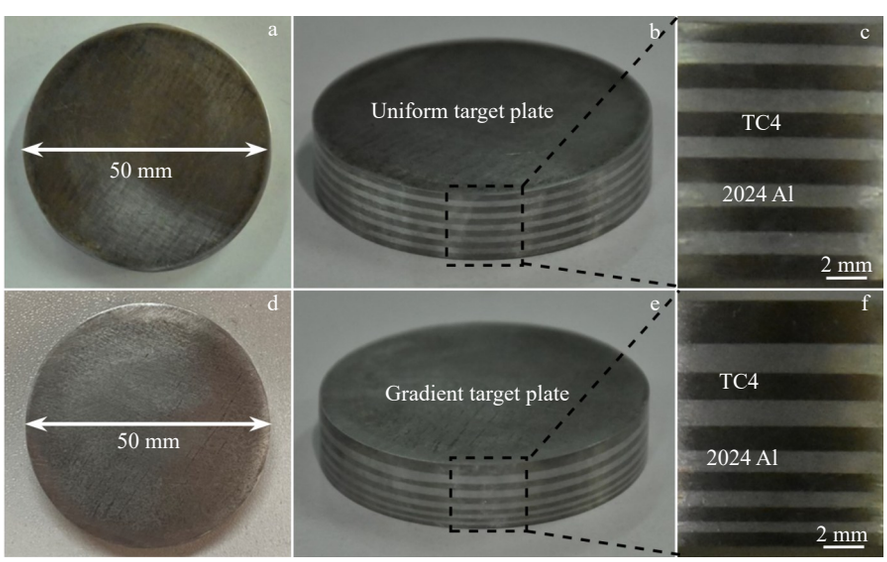

Fig.7 Appearances of uniform target plate (a–c) and gradient target plate (d–f) before penetration

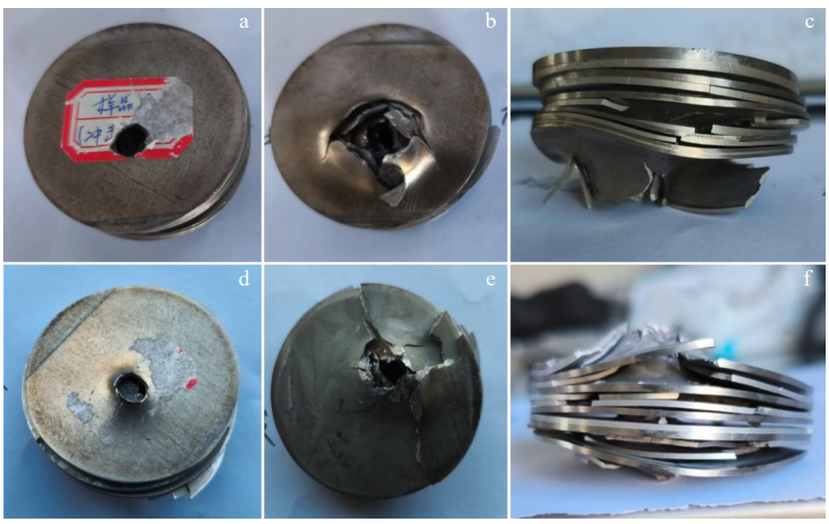

Fig.8 Appearances of gradient target plate (a–c) and uniform target plate (d–f) after penetration

plate, the uniform target plate shows more serious deformation at the bullet hole on the bullet-responsive surface. Besides, the degree of fragmentation is larger than that in the gradient target plate. Compared with that of the gradient target plate, the bullet-responsive surface of the uniform target plate is thinner and less resistant against deformation, resulting in more serious deformation under impact. The slight decrease in bullet velocity by the upper layer leads to greater breakage in the middle and final stages of penetration. This result indicates that the gradient target plate has stronger anti-penetration properties.

4 Discussion

4.1 Optimization mechanism for anti-penetration performance of gradient target plate

In order to analyze the warhead destruction caused by the gradient and uniform target plates, the bullet morphology and stress distribution map during penetration were extracted, as shown in Fig.9 and Fig.10, respectively. The target plate was neglected for simple observation and analysis. The gradient target plate reduces the bullet velocity from 800 m/s to 668 m/s (decrement of 132 m/s) during the early penetration period (50 μs), as shown in Fig. 9b_1. The warhead undergoes serious deformation, which increases the diameter by 0.218 mm. It is worth noting that the maximum effective stress reaches the peak value of 1.886 GPa. At 100 μs, a slight breakage of the warhead occurs, as indicated by the marked regions in Fig.9c_1. The warhead crack results in the stress release, therefore reducing the maximum effective stress value to 1.844 GPa. As the penetration proceeds, the constant friction and extrusion between the warhead and the target plate further intensify the breakage phenomenon. Due to the gradient structure of the target plate, the diameter increment of the warhead is 0.218 and 0.355 mm during impacting at 5 – 50 and 50 – 100 μs, respectively. The growth is rapid in the early and middle stages of the penetration. The maximum effective stress of the warhead decreases from 1.886 GPa to 1.812 GPa, showing a decreasing trend.

Comparing Fig. 9 and Fig. 10, it can be seen that the diameter of the warhead impacting the gradient target plate is 0.114 mm larger than that impacting the uniform target plate at 50 μs. This result suggests that the gradient target plate provides greater impact resistance against the bullet. In the early penetration stage, the gradient target plate provides

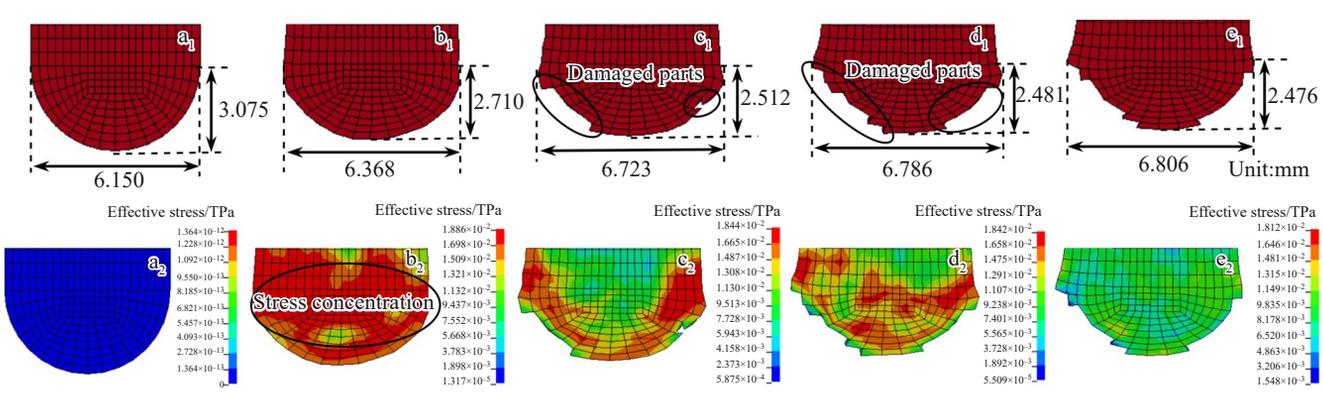

Fig.9 Simulated warhead morphologies (a_1–e_1) and corresponding stress distribution maps (a_2–e_2) of bullet impacting gradient target plate at different moments: (a_1–a_2) 5 μs; (b_1–b_2) 50 μs; (c_1–c_2) 100 μs; (d_1–d_2) 150 μs; (e_1–e_2) 200 μs

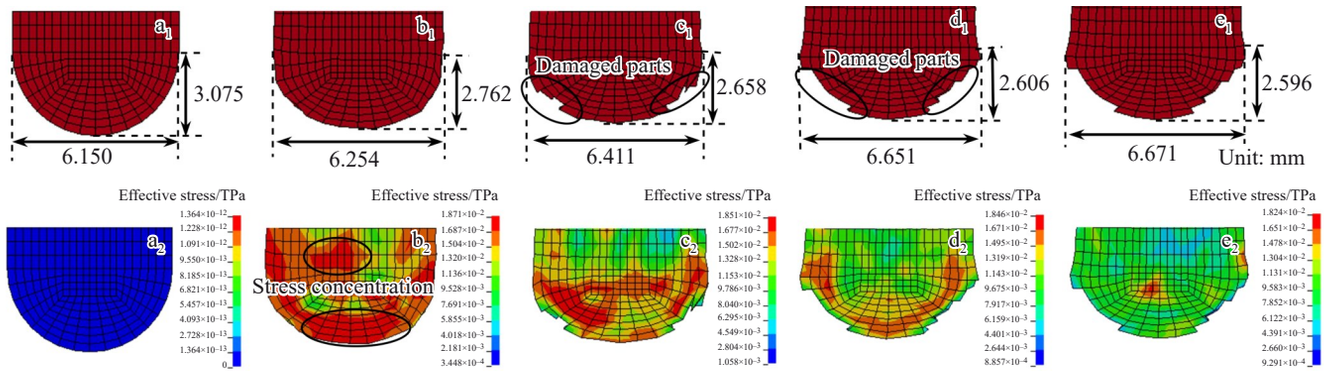

Fig.10 Simulated warhead morphologies (a_1–e_1) and corresponding stress distribution maps (a_2–e_2) of bullet impacting uniform target plate at different moments: (a_1–a_2) 5 μs; (b_1–b_2) 50 μs; (c_1–c_2) 100 μs; (d_1–d_2) 150 μs; (e_1–e_2) 200 μs

greater impact resistance through the larger layer thickness at the upper side and the high titanium alloy percentage, causing the warhead to deform severely. At the same time, the greater deformation of the warhead increases the contact area between the bullet and the target plate, reducing penetration while further increasing impact resistance. Through the analysis of stress distribution map, it is found that the stress concentration also occurs, as indicated by the marked regions in Fig. 10b_2, and the maximum effective stress of the bullet impacting gradient target plate is larger than that impacting uniform target plate by 0.015 GPa. When the bullet impacts the target plate, the impact resistance makes the warhead produce huge stress and strain instantly, and the gradient structure can provide more impact resistance for the target plate. In addition, the velocity of bullets impacting the uniform target plate at 50 μs reduces by 100 m/s (compared with that at 5 μs), and the velocity of bullets impacting the gradient target plate at 50 μs reduces by 132 m/s (compared with that at 5 μs). The deformation degree of warhead, the maximum effective stress values, and the stress distribution all suggest that the gradient target plate provides greater impact resistance against bullet. Greater impact resistance results in a greater reduction in bullet velocity, leading to superior anti-penetration performance of the gradient target plate during the early stages of bullet penetration.

The diameter increment of the warhead is 0.157 and 0.355 mm during impacting at 50–100 μs in the uniform and gradient target plate cases, respectively. The larger diameter further confirms that the gradient target plate provides better anti-penetration performance. The warhead impacting the gradient target plate also shows breakage, as shown in the marked regions of Fig. 10c_1, which is significantly larger than that of the warhead impacting the uniform target plate at the same moment. The breakage effectively reduces the penetration capability of bullet. Warhead breakage produces fragments that are entrapped in the trajectory, increasing frictional resistance and changing the impact direction of warhead, which further reduces the kinetic energy of the bullet. Throughout the penetration process, the warheads impacting the uniform and gradient target plates show different degrees of breakage after impacting for 100 μs. However, the warhead impacting the gradient target plate has a larger area of breakage and produces more debris. The more severe warhead breakage caused by gradient target plate is also beneficial to the anti-penetration performance.

4.2 Stress distribution and crack morphology in gradient target plate

The resistance mechanism of target plate is influenced by many factors, such as target plate structure and stress distribution. To study the effect of gradient structure on the stress distribution during the penetration process, the stress evolution under the condition of initial bullet velocity of 800 m/s was analyzed, and the stress distribution is shown in Fig. 11. The bullet impacts the first layer of TC4 alloy at 16 μs, the stress is concentrated in the gradient target plate at the contact area, as indicated by the marked region in Fig. 11a_2, and the effective stress reaches 1.512 GPa. The total distance of stress transfer in the gradient target plate is 20.0 and 8.7 mm along *X*-axis and *Z*-axis, respectively. The stress transfer along *Z*-axis shows a semi-elliptical diffusion pattern. Stress propagation along *Z*-axis is impeded by the interface, resulting in faster stress transfer along *X*-axis. In addition, the stress propagates from the upper layer to the inner layer at the time scale of microseconds, and the propagation speed is much faster than the bullet penetration speed. Although the first layer of the gradient target plate has not been penetrated yet, the stress has already penetrated through the inner layers of gradient target plate. It is also found that the TC4 layer bears more stress than the 2024 Al layer in the whole gradient target plate. In Ti/Al layered heterostructured materials, the hard-phase layer Ti is still in the elastic state when the soft-phase layer Al already enters the plastic deformation stage. Therefore, the stresses in the material are mainly borne by the hard-phase layer[43]. In this case, TC4 layer bear larger stresses.

At the moments of 50 and 100 μs, the bullet does not penetrate the bottom of gradient target plate. Interestingly, the bottom of gradient target plate shows bending deformation and even localized delamination, which indicates that the cause of the interlayer cracking is not the direct impact of the warhead, as indicated by the marked regions in Fig. 11b_2–11c_2. Interlayer cracking is an important damage form of laminated

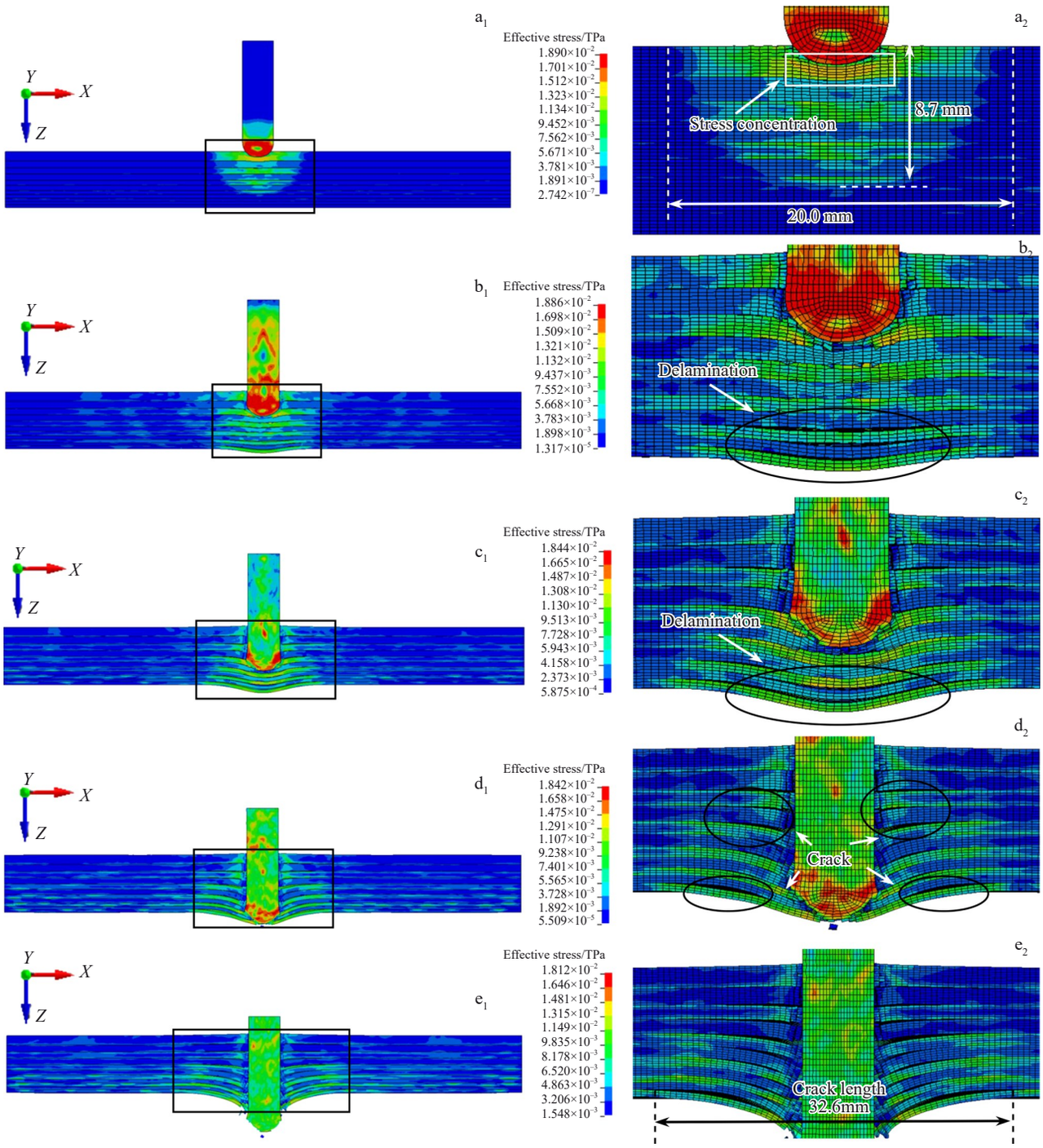

Fig.11 Stress distribution maps (a_1-e_1) and corresponding enlarged maps (a_2-e_2) of bullet impacting gradient target plate at 16 μs (a_1-a_2), 50 μs (b_1–b_2), 100 μs (c_1–c_2), 150 μs (d_1–d_2), and 200 μs (e_1–e_2)

target plate under the impact load of a projectile[44], whereas the stress difference between layers is another important factor leading to delamination of the target plate. The delamination site is marked in Fig. 11b_2, where an obvious stress difference between adjacent layers can be observed. A large amount of stress is generated when the warhead impacts the target plate, and the stress transfer occurs, as shown in Fig. 12. Stress is transmitted and diffused in the target plate in the form of a compressive wave. It travels through the laminated target plate and undergoes transmission and reflection when it encounters the interface[45]. When the compressive wave is transmitted to the interface between the first and second layers, it will be reflected to form a tensile wave and transmitted back to the first layer. At the same time, the tensile wave will be reflected again to form a compressive wave when it encounters the surface. As a result, the first layer of the laminated target plate generates large internal stresses and undergoes bending deformation[46].

The wavefront will undergo one reflection and one transmission for each movement to the interface, and the

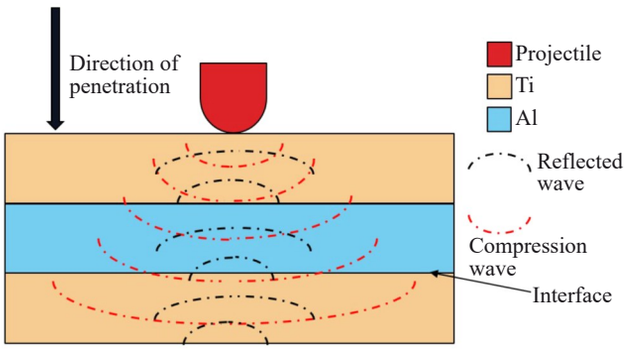

Fig.12 Schematic diagram of propagation of stress wave in laminated Ti/Al material

reflection forms a tensile wave in the opposite direction to the transmitted wave. During the penetration process, the stress waves are continuously transmitted and reflected in the laminated target plate, generating a continuous force until the plate undergoes flexural delamination. In addition, the thickness of the target plate directly affects the intensity of the transmitted wave and the reflection effect to form the tensile wave. The compressive wave passes through thicker target plate with greater intensity decrease, which leads to a weaker intensity of the transmitted wave and the tensile wave[47]. On the contrary, when passing through a thin target plate, the decrease in intensity of compressive wave is less, and the intensities of transmitted and tensile waves are relatively stronger. The upper layer of the gradient target plate barely deforms because it has a large layer thickness, which effectively impedes the compressive wave and produces a smaller reflected wave. At the same time, the large thickness also provides greater deformation resistance for the gradient target plate, so the deformation delamination hardly occurs. The curved delamination at the bottom side of the gradient target plate is caused by the compressive wave that is constantly transmitted and reflected in the target plate. When the compressive wave is transmitted to the interface between the 10th and the 11th layers (the last interface), the bottom thin layer has inferior deformation resistance, so it is difficult to resist the interaction between the compressive wave and the tensile wave. Therefore, deformation and cracks are formed. As the penetration continues, the target plate is continuously compressed and deformed. At the moment of 200 μs, the gradient target plate is completely penetrated. At this time, the bottom thin layer still shows stress concentration, and the gradient target plate shows different degrees of cracking with the longest crack length of 32.6 mm, as shown in Fig.11e_2.

Fig. 13 shows the stress distribution maps of bullet impacting uniform target plate. The stress distribution at 16 μs of bullet impacting uniform target plate is similar to that impacting the gradient target plate, and the distance of stress transfer along *X*-axis is also 20.0 mm. The difference is that the stress propagation distance along *Z*-axis in the gradient target plate is 0.5 mm longer than that in the uniform target plate. Since the interface of laminated composite impedes the wave transmission, and the gradient structure reduces the number of interfaces in the first few layers, the gradient target plate has a faster stress propagation rate in the early penetration stage, which contributes to the uniform dispersion of stress and avoids localized cracking and failure due to stress concentration.

At 50 μs, delamination also occurs at the bottom of the uniform target plate. Unlike the gradient target plate, there is only one interlayer crack. Delamination cracking can also be observed at the upper layer, as indicated by the marked region in Fig.13b_2. As the stress wave is continuously transmitted and reflected in the middle layers, it makes the tensile wave and compressive wave produce a continuous force on the target plate, which causes the plate to bend and delaminate. Uniform target plates lead to delamination bending in both the upper and bottom plates due to the equal thickness distribution. There is no delamination at the upper layer of the gradient target plate, but there are multiple interlayer cracks at the bottom. This is because the upper layer of the gradient target plate is thicker, providing more resistance against deformation, and it is less prone to deformation, which also slows down the failure process of target plate. With the increase in penetration depth, the interlayer cracks are increased gradually. At 200 μs, the gradient target plate is completely penetrated, and cracks are produced in all layers. At the moment of 200 μs, the crack morphology of the uniform target plate is shown in Fig. 13e_2, and the interlayer crack length is 29.0 mm. The gradient target plate has inferior deformation resistance due to the small thickness of bottom layer, and the interlayer crack length reaches 32.6 mm, which is 3.6 mm longer than that in the uniform target plate.

4.3 Energy change of bullet and target plate

Energy absorption capacity is an important index to reflect the protective performance of armor materials. Fig. 14 shows the energy change of the bullet and target plate during impacting with bullet initial velocity of 800 m/s. When the bullet impacts the target plate, the kinetic energy of the bullet decreases, and the internal energy of the target plate increases. The kinetic energy loss of a bullet impacting the gradient target plate is greater, and the internal energy of the gradient target plate increases more obviously. In the first 100 μs of the penetration process, the internal energy of both target plates grows rapidly. Particularly, the internal energy of gradient target plate shows a faster growth rate. This is because in the early stage of penetration, the gradient target plate creates a greater penetration resistance against the bullet, causing more kinetic energy of bullet to be converted into the internal energy of target plate. At 100 – 200 μs, the growth rates of internal energy of both target plates are basically the same. Throughout the penetration process, the energy absorption is 69.7% and 65.5% for the gradient and uniform target plates, respectively. The gradient target plate has a higher ability to dissipate the kinetic energy of the bullet and effectively prevents the bullet from penetrating the target plate. This result again shows that the gradient target plate has better anti-penetration performance.

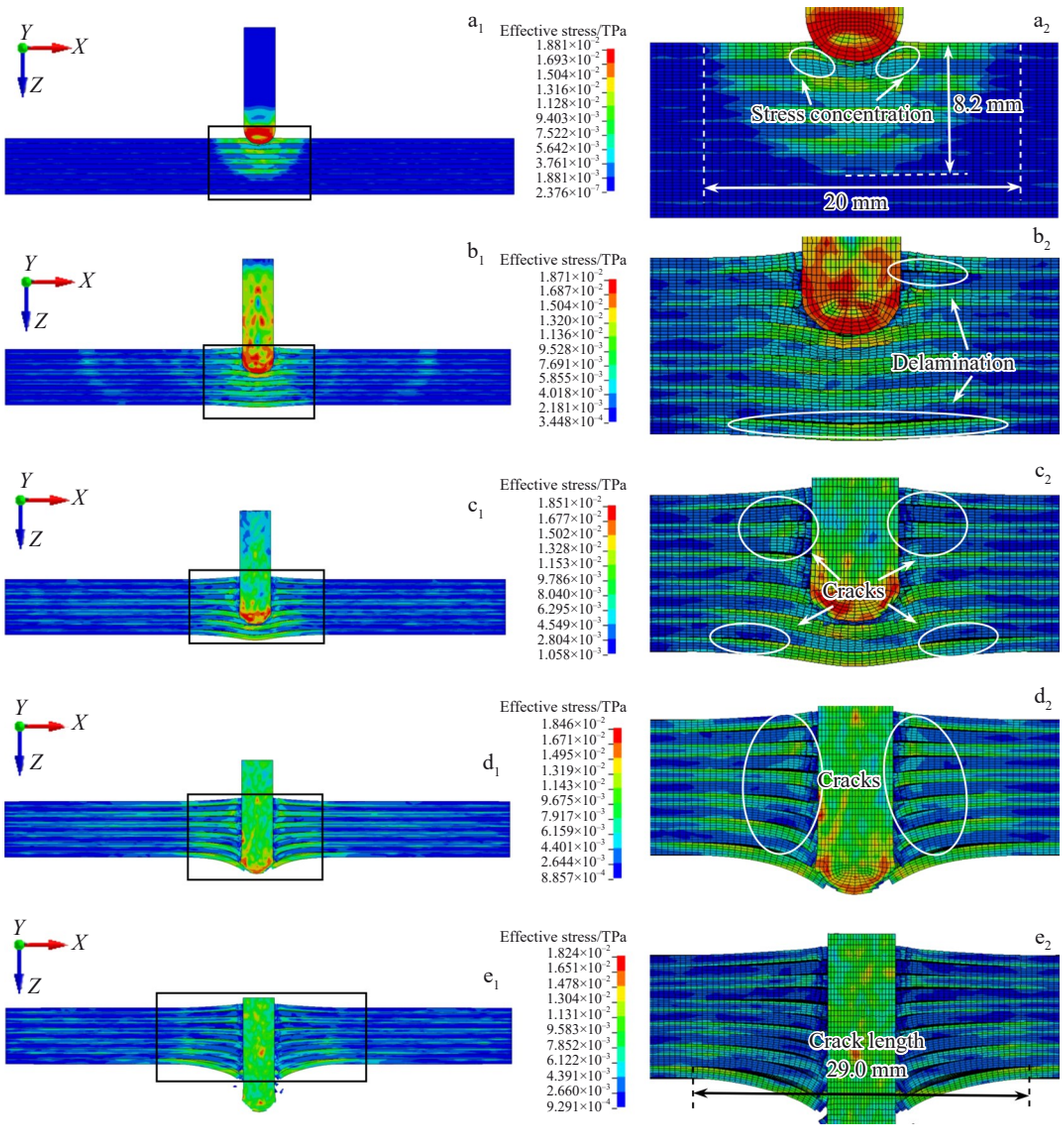

Fig.13 Stress distribution maps (a_1-e_1) and corresponding enlarged maps (a_2-e_2) of bullet impacting uniform target plate at 16 μs (a_1-a_2), 50 μs (b_1–b_2), 100 μs (c_1–c_2), 150 μs (d_1–d_2), and 200 μs (e_1–e_2)

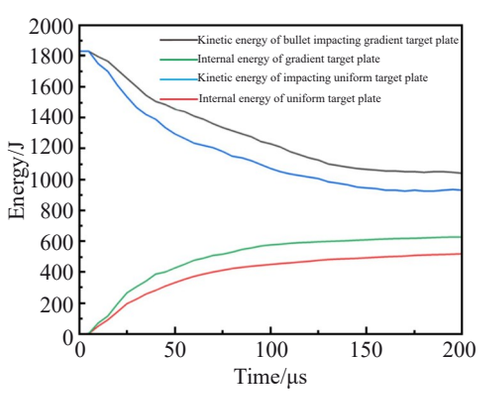

Fig.14 Kinetic energy of bullet and internal energy of target plates

5 Conclusions

1) A finite element simulation was used to simulate and compare the anti-penetration process of the gradient and uniform target plates under different bullet velocities. The gradient structure can effectively improve the anti-penetration performance of laminated target plates.

2) The total thickness of the first four layers of the gradient target plate reaches 5.6 mm, where the titanium content accounts for 50.0% of whole titanium content in the gradient target plate. In this case, the high-level thickness and appropriate percentage of TC4 alloy at the upper side of the gradient structure provide greater impact resistance against the bullet, which increases the warhead breakage and enhances the anti-penetration performance.

3) The interface of laminated composite materials hinders the transmission of stress waves, and the gradient structure reduces the number of interfaces at the upper layers of the target plate, which promotes uniform dispersion of stress, therefore avoiding localized cracking and failure due to stress concentration.

4) Interlayer cracking occurs in both gradient and uniform

target plates due to continuous transmission and reflection of stress waves. The gradient target plate reduces the stress waves more effectively due to the thicker layer thickness at the upper side, thus slowing down the destruction of the target plate.

5) Throughout the penetration process, the energy absorption is 69.7% and 65.5% for the gradient and uniform target plates, respectively. The gradient target plate consumes more kinetic energy of the bullet, therefore effectively preventing the penetration of the bullet into the target plate.

References

1 Dong Y L, Zi F, Yang L H *et al*. *Mechanics of Advanced Materials and Structures*[J], 2022, 29(28): 7035

2 Su L C, Yi C H, Liu W J *et al*. *Journal of Ordnance Equipment Engineering*[J], 2018, 39(1): 157

3 Bao Y G, Gao X J, Wu Y C *et al*. *Journal of Physics: Conference Series*[J], 2021, 1855: 012035

4 Mo T Q, Chen J, Chen Z J *et al*. *Materials Characterization*[J], 2020, 170: 10731

5 Yu M R, Zhao H Y, Jiang Z H *et al*. *Journal of Materials Science & Technology*[J], 2019, 35(8): 1543

6 Zhao Yuhong, Jing Jianhui, Chen Liwen *et al*. *Acta Metall Sin*[J], 2021, 57(9): 1107 (in Chinese)

7 Lyu S Y, Sun Y B, Ren L *et al*. *Advanced Engineering Materials*[J], 2017, 19(8): 1700070

8 Liang F, Wang Z X, Luo Y W *et al*. *Acta Materialia*[J], 2021, 216: 117138

9 Wang T, Liu W L, Liu Y M *et al*. *Journal of Materials Processing Technology*[J], 2021, 295: 117157

10 Li M X, Li H Q, Liu Y H *et al*. *Materials Science and Engineering A*[J], 2023, 884: 145562

11 Zhang Danning, Meng Linggang, Yang Yang *et al*. *Special Casting & Nonferrous Alloys*[J], 2024, 42(10): 1242 (in Chinese)

12 Bai S, Wei L, He C *et al*. *Journal of Materials Research and Technology*[J], 2022, 21: 1013

13 Wang D, Liu Q, Wan H Q *et al*. *International Journal of Applied Ceramic Technology*[J], 2023, 20(6): 3608

14 Wang W R, Xie H F, Xie L *et al*. *International Journal of Minerals, Metallurgy, and Materials*[J], 2018, 25: 1320

15 Zhang B, Zhong Z X, Ye J *et al*. *Ceramics International*[J], 2020, 46(7): 9957

16 Zhang Q H, Li J G, Ren T F *et al*. *Journal of Materials Research and Technology*[J], 2023, 26: 5236

17 Shi Mingdong, Yuan Meini, He Xiaojing *et al*. *Acta Materiae Compositae Sinica*[J], 2018, 35(8): 2286 (in Chinese)

18 Zhao Y H. *npj Computational Materials*[J], 2023, 9(1): 94

19 Chen L Q, Zhao Y H. *Progress in Materials Science*[J], 2022, 124: 100868

20 Zhao Y H, Xin T Z, Tang S *et al*. *MRS Bulletin*[J], 2024, 49: 613

21 Zhao Y H. *Materials Genome Engineering Advances*[J], 2024, 2(2): e44

22 Guo Q W, Hou H, Wang K L *et al*. *npj Computational Materials*[J], 2023, 9(1): 185

23 Xin T Z, Zhao Y H, Mahjoub R *et al. Science Advances*[J], 2021, 7(23): eabf3039

24 Xin L, Yuan M N, Yao Y H *et al. Materials Research Express*[J], 2019, 6(8): 0865f8

25 Liu W, Zhao Y H, Zhang Y T *et al. International Journal of Plasticity*[J], 2023, 164: 103573

26 Kuang W W, Wang H F, Li X *et al*. *Acta Materialia*[J], 2018, 159: 16

27 Zhang J B, Wang H F, Kuang W W *et al*. *Acta Materialia*[J], 2018, 148: 86

28 Cai X M, Zhang W, Wang J Y *et al*. *Thin-Walled Structures*[J], 2024, 199: 111840

29 Sharma A, Mishra R, Jain S *et al*. *Thin-Walled Structures*[J], 2018, 126: 193

30 Li T Z, Grignon F, Benson D J *et al*. *Materials Science and Engineering A*[J], 2004, 374(1–2): 10

31 Yuan M N, Yao Y H, Han F Z *et al*. *Results in Physics*[J], 2020, 18: 103308

32 Zou Y C, Xiong C, Yin J H. *Science and Engineering of Composite Materials*[J], 2021, 28(1): 372

33 Senthil K, Iqbal M A, Arindam B *et al*. *Thin-Walled Structures*[J], 2018, 126: 94

34 Akbari T, Ansari A, Pishbijari M R. *Ceramics International*[J], 2023, 49(19): 30937

35 Li M X, Wang K L, Guo Q W *et al*. *Materials Science and Engineering A*[J], 2024, 901: 146347

36 Li H, Zong S Z, Xiong X Y. *International Journal of Impact Engineering*[J], 2023, 182: 104780

37 Qi Zichen, Yu Chao, Xiao Hong *et al*. *Chin J Nonferrous Met*[J], 2018, 28(6): 1120 (in Chinese)

38 Ahn J H, Nguyen K H, Park Y B *et al*. *International Journal Aeronautical and Space Sciences*[J], 2010, 11(3): 221

39 Deng Y G, Wang Y, Qu K F *et al*. *Structures*[J], 2022, 45: 542

40 Wu Y D, Wang X D, Ma M H *et al*. *Ceramics International*[J], 2023, 49(24): 39800

41 Yungwirth C J, O'Connor J, Zakraysek A *et al*. *Journal of the American Ceramic Society*[J], 2011, 94: s62

42 Shuai C, Liu W, Li H Q *et al*. *International Journal of Plasticity*[J], 2023, 170: 103772

43 Huang M, Xu C, Fan G H *et al. Acta Materialia*[J], 2018, 153: 235

44 Shi Y, Pinna C, Soutis C. *Composite Structures*[J], 2014, 114: 10

45 Wang Y, Liu Q, Zhang B *et al*. *Materials Science and Engineering A*[J], 2023, 874: 145071

46 Li Y M, Zhang H, Yuan M N. *Frontiers in Materials*[J], 2022, 9: 806020

47 Li R, Huang Z X, Zu X D *et al*. *Explosion and Shock Waves*[J], 2018, 38(5): 1039

梯度层厚度对2024 Al/TC4层压复合材料抗侵彻性能的影响

王康安[1]，李沐奚[1]，侯　华[1,2]，赵宇宏[1,3,4]

(1. 中北大学 材料科学与工程学院 教育部与山西省高性能铝镁合金材料协同创新中心，山西 太原 030051)

(2. 太原科技大学 材料科学与工程学院，山西 太原 030024)

(3. 北京科技大学 材料基因组工程创新中心，北京 100083)

(4. 辽宁材料研究院 材料智能技术研究所，辽宁 沈阳 110164)

摘　要：将梯度结构引入金属叠层靶板，通过有限元仿真对梯度结构与均匀层厚靶板进行抗侵彻模拟对比，并通过冲击实验验证分析。结果表明，梯度结构前端的高层厚及合适的Ti合金占比为子弹带来更大的冲击阻力，使弹头镦粗破损加剧，提升抗侵彻性能。此外，在冲击过程中，应力以波的形式在靶板各层透射和反射，压缩波与拉伸波相互作用使靶板产生非协同形变并导致分层。梯度靶板凭借更高的能量吸收率，消耗了子弹更多的动能，使得抗侵彻性能更进一步。本研究为梯度结构在金属叠层装甲中的应用提供了理论依据。

关键词：梯度结构；层压复合材料；有限元模拟；抗侵彻机理

作者简介：王康安，男，1999年生，硕士生，中北大学材料科学与工程学院教育部与山西省高性能铝镁合金材料协同创新中心，山西 太原　030051，E-mail：1308434934@qq.com